Design and Numerical Analysis of Wind Turbine for Energy Recovery in Electric Vehicles

Emin El [a1], Cengiz Yildiz [b], Besir Dandil [c], and Ahmet Yildiz [d]

[a] *Department of Mechanical Engineering, Faculty of Engineering and Architecture, Bitlis Eren University, Bitlis, Türkiye*
[b] *Department of Mechanical Engineering, Faculty of Engineering, Fırat University, Elazig, Türkiye*
[c] *Department of Mechatronics Engineering, Faculty of Engineering and Natural Sciences, Iskenderun Technical University, Hatay, Türkiye*
[d] *Department of Mechatronics Engineering, Faculty of Engineering, Fırat University, Elazig, Türkiye*

ABSTRACT

In this study, a design for a horizontal-axis wind turbine was created to recover some of the energy lost by moving vehicles and turn it into electrical energy, and its effectiveness was examined using computer simulations. The geometry of the wind turbine system was modeled using SolidWorks software. The CFD simulation study was carried out using the SST k-ω turbulence model. ANSYS Fluent commercial software was used in the simulations. The initial inlet velocity was taken at three different values of 10 m/s, 15 m/s and 27 m/s, respectively. The results obtained indicate that the designed wind turbine has the potential to generate power for an electric vehicle. In the designed vehicle-type wind turbine system, it has been determined that an efficient blade design and consequent improvement of airflow characteristics will increase the generated electrical power and reduce the additional impact on vehicle aerodynamics. Furthermore, the position of the designed wind turbine on the vehicle significantly influences the vehicle's aerodynamics. It has been determined that positioning the wind turbine in a way that increases the vehicle's projection area may lead to an increase in the aerodynamic losses of the vehicle.

Keywords: Electric Vehicle, Energy Recovery, Wind Energy, Wind Turbine, Aerodynamics, Efficiency.

1. INTRODUCTION

In the late 19th century, the discovery of electricity and the magnetic field led to the emergence of the first electric motor-driven vehicles. The introduction of cars powered by internal combustion engines (ICE) that used fossil fuels occurred around the same time. During the world wars, technology for vehicles powered by internal combustion engines rapidly developed due to their long range and the ready availability of fuel, despite the engines being noisy and significantly polluting the air. Accordingly, interest in electric vehicles (EVs) started to decrease in the 1910s due to the technological inadequacies of the period [1].

Today, factors like limited fossil fuel reserves, rising fuel costs, global warming, environmental pollution, and emission restrictions make electric vehicles more appealing to both manufacturers and consumers every day [1]. Electric vehicles operate with electrical energy stored in batteries, fuel cells, and ultracapacitors, which is generated from conventional production facilities and renewable energy sources. Therefore, electric vehicles are highly dependent on energy storage technologies [2–4]. The electrical energy stored in batteries and other storage systems is used for the operation of the vehicle's electric motor and essential systems. To meet the additional energy demand from electric vehicles, many countries are investing in renewable energy systems, such as solar and wind [5–7].

Electric motors provide the movement in electric vehicles. Batteries, which store electrical energy and do not require the combustion of any fuel, provide the necessary movement energy. As a result, the vehicle produces no emissions [8]. Additionally, the torque and efficiency of electric motors are higher compared to internal combustion engines, easier to control, and have better performance. It has also led

[1] Corresponding author: eel@beu.edu.tr

to the emergence of autonomous and intelligent driving technologies with their easy and high-performance control features. Despite all these superior features of electric vehicles, their purchasing costs are high and their range is relatively low due to problems with energy storage. This situation is an important problem for electric vehicles today and restricts their widespread use. Thus, new methods have to be developed to enhance the range of electric cars [9–12].

The use of renewable energy sources is important for the supply of energy required in electric vehicles. Due to the fact that solar energy, a renewable energy source, depends on weather conditions, has low efficiency, and requires large areas, the widespread use of such systems, especially in vehicles, is not currently considered feasible. Therefore, by using environmentally friendly wind turbine systems for electricity generation in vehicles that operate continuously and efficiently, we can solve the range problem by increasing the vehicle's energy efficiency.

Research into the range issues of electric vehicles has mostly focused on reducing energy consumption and recovering some of the energy lost. Energy recovery systems enable the conversion of dissipated energy into electricity, which can then be used for several purposes. Studies on energy recovery technologies in electric cars typically concentrate on regenerative braking, vibration energy recovery, and waste heat recovery [11,13]. However, there are very few studies on wind turbine systems designed for vehicles.

According to research, 8%–40% of the braking energy of an EV in urban traffic can be recovered by regenerative braking (RB) [14,15], while roughly 30%–50% of its total energy is lost on friction braking (FB) [16]. The fuel efficiency enhancement for a conventional passenger vehicle equipped with regenerative suspension was reported to be between 2 and 3 percent, whereas the figures for electric vehicles range from 7 to 10 percent. During the driving cycle, 30% to 47% of the energy sent to the wheels is dissipated owing to wind resistance [17]. The following presents studies on wind energy recovery found in the literature.

H. Begum and M.A. Hossain [18] proposed the use of wind turbines mounted on vehicles to address the range issue in electric vehicles. They asserted that wind energy can be utilized to recharge batteries while vehicles are in motion. Z.A. Khan et al. [19] conducted a numerical investigation on the aerodynamic drag and air velocity characteristics of a vehicle equipped with a wind turbine. In their study, they emphasized that designing a wind turbine for harnessing wind energy around electric vehicles and positioning it on the front bumper of the vehicle would create a more effective charging system. E. El et al. [20] conducted a numerical investigation into how placing a wind turbine on the front bumper of the vehicle affects the vehicle's aerodynamic performance and energy efficiency. The research explored the impact of a vehicle-mounted wind turbine on a car traveling 100 km at a consistent speed of 27 m/s. The results showed a total energy loss of 2.47% in the wind turbine-equipped vehicle model (M2) compared to the basic vehicle model (M0). Nevertheless, the wind turbine yielded a net energy gain of 5.13%, indicating that the turbine's energy gain was greater than its energy loss. H. Fathabadi [21] investigated the possibility of utilizing a wind turbine to recapture some of the kinetic energy losses of a car. In this context, he placed a small wind turbine behind a car's capacitor to recover some of the kinetic energy of the wind passing through the capacitor. The experimental data obtained in the study showed that the use of the wind turbine increased the electric vehicle driving range and the power efficiency of the power supply by 6.4 km and 0.2%, respectively. G.A. Anagie et al. [22] studied the performance of a tiny horizontal-axis wind turbine mounted on the roof of a pickup truck. The study's goal was to charge the vehicle's batteries using power provided by the wind turbine. According to the findings of the study, the highest powers derived from the experimental and theoretical studies were 334 W and 437 W, respectively, at a maximum vehicle speed of 25 m/s and a reaction wind speed of 28.6 m/s. M.S.Y. Ebaid et al. [23] aimed to generate electricity by utilizing the air circulating around the moving vehicle through micro-wind turbines (MWTs). In this way, they aimed to increase the efficiency and range of the vehicle. They analyzed the performance of the designed vehicle model in three driving cycles, including urban, high-dynamic, and highway driving scenarios. The results showed that adding micro-wind turbines makes the engine 8.38% more efficient for the highway drive cycle (FTP), 4.6% more efficient for the new European drive cycle (NEDC), and 1.01% more efficient for the standardization random test aggressive drive cycle (RTS). M.C.F. Nguefack et al. [24] employed a 3D numerical simulation to investigate the influence of bull bars and Savonius wind turbines on the aerodynamic characteristics of an SUV vehicle. The first findings indicate that both the vehicle in its original state and the vehicle equipped with bull bars exhibit identical flow characteristics.

Subsequently, it was shown that the modified Savonius Bach model yielded drag coefficient values of 0.402, 0.403, and 0.404 for angles of 30°, 80°, and 120°, respectively.

In this study, a vehicle-type horizontal-axis wind turbine was designed and numerically analyzed to recover some of the energy losses in moving vehicles as electrical energy. The literature review did not find any similar studies. In this original study, the geometry of the wind turbine that can be mounted on the vehicle was designed using SolidWorks software. Pressure contours, velocity vectors, and streamlines of the designed wind turbine model at vehicle speeds of 10 m/s, 15 m/s, and 27 m/s were determined, and the obtained results were presented. The CFD simulation study was carried out using the SST k-ω turbulence model. ANSYS Fluent commercial software was used in the simulations.

2. WIND TURBINE DESIGN AND NUMERICAL ANALYSIS

In order to realize the wind turbine design, the design parameters must first be determined. These parameters are: the amount of power received from the wind (P), the power coefficient (C_p), the number of blades (z), the tip-speed ratio (λ_D), the blade stiffness ratio (σ), and the and the turbine blade structure [25,26].

2.1. Calculation of the Amount of Power Received from The Wind

The wind turbine to be placed in the front section of the vehicle is designed so that it does not change the vehicle's projection area, and the area swept by the turbine blades is maximized. In the examinations of the front part of the model vehicle, it was determined that the maximum diameter for the wind turbine to be placed on the vehicle could be 0.50 m. Equation 1 calculates the maximum power that the wind turbine can produce in this case [27–29].

$$P_T = \frac{1}{2}\rho A V^3 C_p \tag{1}$$

In the power calculation performed, the power coefficient (Betz limit) C_p=0.5926, air density ρ=1.225 (kg/m^3), swept area of the blade A=πR^2 (m^2), and wind speed V (m/s) are taken as 10 m/s, 15 m/s, and 27 m/s, respectively.

2.2. Number of Blades

One of the fundamental parameters influencing wind turbine design is the number of blades. As the number of blades increases, the amount of power to be obtained from the turbine and turbine efficiency increase, while the angular velocity of the blade and the beam length decrease. Additionally, an increase in the number of blades in wind turbines leads to higher turbine costs. Three-bladed wind turbines are more economical and aesthetically pleasing than others, which has led to their wider use [25].

2.3. Tip Speed Ratio

Tip speed ratio is a crucial parameter in wind turbines, which is determined by dividing the speed of the blade's tip by the velocity of the fluid [30]. The tip speed ratio (λ_D) in single-blade wind turbines, where the blades rotate at high speeds, between 6 and 20, while in three-blade wind turbines, the tip speed ratio is generally between 5 and 8. Equation 2 is used to calculate the blade tip speed ratio [30–32].

$$\lambda_D = \frac{\Omega R}{V} \tag{2}$$

The equation defines the variables as follows: λ_D represents the tip speed ratio, Ω (r/s) represents the angular velocity of the wind turbine blade, R (m) represents the radius of the turbine blade, and V (m/s) represents the wind speed.

2.4. Selection Airfoils for Wind Turbine Blades

The airfoils used in wind turbine blades consist of a combination of two special curves passing over and under the chord line (Figure 1).

In these curves, the term "camber" is used to describe a situation where the radius of curvature of the upper curve is smaller than that of the lower curve. The camber induces the formation of different flow velocities on both surfaces of the blade. The varied flow velocities on the blade surfaces create a pressure difference between the upper and lower surfaces, generating a lift force (F_l) from the lower part to the upper part of the blade. The force that occurs in the direction parallel to the flow velocities is called the drag force (F_d). These forces are the forces that enable energy to be obtained from the wind turbine [33]. Lift and drag forces are expressed as in Equations 3 and 4, respectively.

$$F_l = \frac{1}{2}\rho A V^2 C_l \tag{3}$$

$$F_d = \frac{1}{2}\rho A V^2 C_d \tag{4}$$

The performance of the wind turbine blade airfoil is related to the lift (C_l) and drag (C_d) force coefficients, which are two important dimensionless coefficients. The C_l/C_d ratio determines the aerodynamic performance [34]. In the design, the drag coefficient is much smaller compared to the lift coefficient ($C_d << C_l$) since it is assumed that the aerodynamic blade airfoil operates closely to the best lift-to-drag ratio.

In wind turbine design, the most commonly used blade profiles today are the NACA series airfoils. A typical NACA airfoil and its basic dimensions are given in Figure 2.

NACA airfoils are characterized by parameters such as chord length (c), maximum thickness (d), maximum camber (f), position of maximum thickness (X_d), position of maximum camber (X_f), radius of curvature of the leading edge (r_N), upper curve form $y_u(x)$, and lower curve form $y_o(x)$. The dimensionless maximum thickness ratio ($\bar{d}$) and dimensionless maximum camber ratio ($\bar{f}$) in these airfoils are expressed as Equation 5 and Equation 6, respectively [35,36].

$$\bar{d} = \frac{d}{c} \tag{5}$$

$$\bar{f} = \frac{f}{c} \tag{6}$$

Each number digit in the NACA airfoil codes has a different meaning. In a four-digit NACA airfoil, the first digit indicates the maximum camber ratio (%), the second digit (multiplied by 10) indicates the position of the maximum camber from the leading edge (%), and the last two digits indicate the maximum thickness ratio (%) of the airfoil.

2.5. Calculation of Optimal Chord Length and The Blade Twist Angle

In order to create the wind turbine blade model, it is essential to determine the number of blades, tip-speed ratio, airfoil type, angle of attack for the blade airfoil, lift, and drag coefficients. Depending on these, parameters such as chord length and twist angle should be calculated. While making these calculations, the angle of attack (α) and C_l/C_d ratios should be carefully selected. A small angle of attack is preferable, while the C_l/C_d ratio should be selected at its maximum value. In the study, a three-bladed ($Z = 3$) wind turbine was selected, and the NACA0009 airfoil was preferred (Figure 3).

Calculations performed using the XFOIL program revealed that the NACA0009 airfoil has the maximum C_l/C_d ratio at a 3.75° angle of attack. Therefore, the calculations were conducted at a design angle of attack of 3.75°. Table 1 provides the variations in the C_l/C_d ratio with respect to angles of attack.

The chord length and the blade twist to be created with the NACA0009 airfoil (λ_D=5, Z=3, R=0.25, α_A=3.75°) at the determined sections were calculated using Equation 7 and Equation 8, respectively [38].

$$C(r) = \frac{1}{z}\frac{16\pi r}{c_l} sin^2\left(\frac{1}{3} arctan\left(\frac{R}{\lambda_D r}\right)\right) \quad (7)$$

$$\beta(r) = \frac{2}{3} arctan\left(\frac{R}{\lambda_D r}\right) - \alpha_A(r) \quad (8)$$

The calculated values are provided in Table 2. The r (m) in Table 2 represents the distance of the blade element from the blade root. Blade model calculations were performed at 10 different distances (sections).

2.6. Blade Solid Model Creation

SolidWorks software was used for solid modeling of the blade after the blade twist angle and chord length were calculated. In the first stage, 10 different planes, evenly spaced and parallel to the front plane, were created, and these planes were referred to as sections (Figure 4). Then, NACA0009 airfoils were placed in these sections according to the calculated blade twist angle and chord lengths. The front and isometric views of the airfoils before solid modeling are shown in Figures 5 and 6.

Figure 6 shows an isometric view of the NACA0009 airfoil generated with the values calculated for λ_D=5, Z=3, R=0.25, and α_A=3.75° design conditions. It also shows the solid model of the blade without the root connection.

The solid model of the three-bladed turbine designed for 0.50 m diameter and clockwise rotation with the NACA0009 airfoil is given in Figure 7.

2.7. Solution Geometry

The size of the computational domain was defined by considering the length (L) and diameter (D) of the wind turbine. The dimensions were created with a space two times the turbine diameter in front of the wind turbine, eight times behind, and two times above, below, and on the sides. To achieve a consistent convergence of the simulation result (Figure 8), the length from the back of the vehicle model to the exit (8D) is provided.

2.8. Mesh Structures

The mathematical mesh process is crucial for obtaining accurate results in the analyses conducted. The use of a coarse mesh structure may not yield efficient results for the solution. Additionally, as the element sizes decrease in the mathematical meshing process, the analysis solution time increases. The surface of the full-scale wind turbine is divided into triangular elements (Figure 9). Additionally, a study on grid independence was undertaken in order to ascertain that the size of the elements does not have an impact on the outcomes. The analysis focused on the variation in drag coefficient across three distinct mesh structures: a coarse mesh consisting of 2732647 elements, a medium mesh including 3678920 elements (as seen in Figure 10), and a fine mesh consisting of 4625299 components. Grid independence studies have shown that the drag force converges to the number of nodes (638521 and 3678920).

2.9. Boundary Conditions and Solution Settings

The reference values, boundary conditions, and solution settings to be used in the analysis of the designed wind turbine model are given in Table 3.

3. RESULTS AND ANALYSES

Analyses were performed in this section using Ansys-Fluent software at three distinct velocities of 10 m/s, 15 m/s, and 27 m/s for the designed wind turbine model. In the analyses, values obtained for static pressure contours, velocity contours, and streamlines of wind turbine blades are presented.

In the analyses, it was determined that the highest pressure occurs in the central regions shown in red when considering the side of the blade facing the wind primarily, gradually decreasing towards the edges during turbine operation. Negative pressure zones were observed at the rear of the blade. The negative pressure regions of the blade are referred to as suction surfaces, while the regions with positive pressure are referred to as compression surfaces. The wind turbine blade rotates due to the pushing force of the pressure surface and the pulling force of the suction surface. The highest pressure on the wind turbine blade was found to be 96.82 Pa, 171.8 Pa, and 483.8 Pa at wind speeds of 10 m/s, 15 m/s, and 27 m/s, respectively. The minimum pressure was calculated to be -204.6 Pa, -394.6 Pa, and -1223.0 Pa, respectively. The isometric, front and side perspectives of the static pressure contours of the developed turbine model depending on the wind speed are shown in Figure 11.

When examining the velocity vector distribution of the wind turbine model, it was determined that the highest velocity occurs in the regions shown in red, while the lowest velocity occurs in the regions shown in blue. At wind speeds of 10 m/s, 15 m/s, and 27 m/s, the maximum velocity value in the rear regions of the wind turbine according to the wind flow direction is calculated to be 18.98 m/s, 26.07 m/s, and 43.95 m/s, respectively. Figure 12 depicts the isometric, frontal, and lateral perspectives of the velocity vector distribution of the wind turbine model.

When examining the streamlines of the wind turbine model, it was observed that the airflow accelerates on the suction surface of the blade profile while decelerating on the pressure surface as the air flows over the blade. This situation creates a pressure difference between the two surfaces. It was determined that this pressure difference causes air movement from the compression surface to the suction surface at the tip of the blade, and as a result of the combination of these air movements with the flow, tip vortices are formed. The streamline dispersion of the wind turbine model is depicted in Figure 13, isometric, front, and side perspectives.

If the wind turbine blade design is used in vehicles, it is calculated that it can generate 1400.28 W for 27 m/s speed, 200.10 W for 15 m/s speed, and 71.14 W for 10 m/s speed.

4. CONCLUSION

In this study, a new wind turbine model was designed with the aim of recovering a portion of the losses incurred due to air movement at specific speeds in land vehicles as electrical energy and offsetting a part of the energy required during the vehicle's motion. An investigation was conducted into the impact of the designed wind turbine on the vehicle at velocities of 10 m/s, 15 m/s, and 27 m/s. In this context, a wind turbine model was created using SolidWorks software. In the study, computational fluid dynamics (CFD) simulations were performed using the SST k-ω turbulence model. Numerical simulations employed ANSYS-Fluent software. In the analysis, the motion of the wind turbine is taken into account. The results obtained are summarized as follows.

The NACA0009 airfoil was used in the wind turbine design. The calculations reveal that the NACA0009 airfoil achieves its maximum *Cl*/*Cd* ratio at a 3.75° angle of attack. At this angle of attack, the lift coefficient (C_l) value was calculated as 0.4557, and the drag coefficient (C_d) value was calculated as 0.00992.

The analyses of the designed and solidly modeled wind turbine show that the highest pressure on the side of the blade exposed to the wind occurs in the middle parts and gradually decreases toward the edges. On the rear sides of the blade, negative pressure zones have been observed. As the vehicle speed

increases, it has been determined that high pressure, low pressure, and velocity values increase in the blade region. When the airflow passes over the blade, it has been observed that the speed increases on the suction surface of the blade profile, while it slows down on the pressure surface. It has been determined that this situation creates a pressure difference between the two surfaces. This pressure difference at the tip of the blade induces airflow from the pressure surface to the suction surface, and the merging of these airflow movements results in the formation of tip vortices.

The highest pressure on the wind turbine blade was found to be 96.82 Pa, 171.8 Pa, and 483.8 Pa at wind speeds of 10 m/s, 15 m/s, and 27 m/s, respectively. The minimum pressure was calculated to be -204.6 Pa, -394.6 Pa, and -1223.0 Pa, respectively.

When examining the velocity distribution around the wind turbine model at speeds of 10 m/s, 15 m/s, and 27 m/s, the maximum speed found at the back of the turbine, based on the wind direction, was 18.98 m/s, 26.07 m/s, and 43.95 m/s, respectively.

As a result, the conducted analyses indicate that the designed wind turbine has the potential to generate power in the range of 71.14 W to 1400.28 W, depending on the vehicle speed for an electric vehicle. Efficient blade design in the proposed vehicle-type wind turbine system, along with the improvement of airflow characteristics, will enhance the generated electrical power and reduce the additional impact on vehicle aerodynamics. The wind turbine's position on the vehicle was also important for vehicle aerodynamics when the pressure and speed contours were examined.

ACKNOWLEDGMENT

This work has been derived from the PhD research conducted by E. EL. The authors express their gratitude to the Scientific Research Projects Coordination Unit (FUBAP) of Fırat University Rectorate for their financial support under project number MF.20.38.

BIOGRAPHIES

Emin EL was born in Diyarbakır, Türkiye in 1985. He received his B.Sc. degree in Mechanical Engineering from Dicle University in 2008. He received his M.Sc. and Ph.D. degrees in Mechanical Engineering from Firat University in 2013 and 2023, respectively. Between 2013 and 2024, he worked as a lecturer at the Vocational School of Technical Sciences of Bitlis Eren University, Bitlis, Türkiye. Since 2024, he has been serving as an assistant professor in the Department of Mechanical Engineering at the Faculty of Engineering and Architecture, Bitlis Eren University. His research interests include thermodynamics, heat transfer, electric vehicles, solar stills, and renewable energy sources.

Cengiz Yildiz was born in Elazig, Türkiye, in 1962. He is currently a Professor in the Department of Mechanical Engineering at Firat University, Elazig, Türkiye. He received his B.Sc., M.Sc. and Ph.D. degrees in Mechanical Engineering from Firat University in 1985, 1987 and 1990, respectively. His research interests include thermodynamics, heat transfer, heat exchangers, and renewable energy sources.

Ahmet Yildiz received his B.Sc. degrees in Electrical and Electronics Engineering and Mechatronics Engineering (double major) from Firat University, Elazig, Türkiye, in 2015. He received his M.Sc. and Ph.D. degrees in Mechatronics Engineering from Firat University in 2018 and 2023, respectively. He is currently an Assistant Professor with the Department of Mechatronics Engineering at Firat University, Elazig, Türkiye. His research interests include electric machine design and applications, renewable energy systems, and mechatronics.

Besir Dandil is currently a Professor in the Department of Mechatronics Engineering at Iskenderun Technical University, Hatay, Türkiye. He received his B.Sc., M.Sc. and Ph.D. degrees in Electrical and Electronics Engineering from Firat University, Elazig, Türkiye, in 1992, 1998 and 2004, respectively. His current research interests include analogue and digital electronics, the power electronics, power quality, and control systems.

REFERENCES

[1] Edgerton, D., “The electric vehicle: technology and expectations in the automobile age”, The Economic History Review, 58(1), pp. 224–225 (2005). https://doi.org/10.1111/j.1467-8519.2005.00302_27.x.

[2] Lukic, S. M., Jian C., Bansal, R. C., et al. “Energy Storage Systems for Automotive Applications”, IEEE Trans. Ind. Electron., 55(6), pp. 2258–2267 (2008).

https://doi.org/10.1109/TIE.2008.918390.
[3] Chau, K. T., Wong, Y. S., and Chan, C. C., "An overview of energy sources for electric vehicles", Energy Conversion and Management, 40(10), pp. 1021–1039 (1999). https://doi.org/10.1016/S0196-8904(99)00021-7.
[4] Hannan, M. A., Azidin, F. A., and Mohamed, A., "Hybrid electric vehicles and their challenges: A review", Renewable and Sustainable Energy Reviews, 29, pp. 135–150 (2014). https://doi.org/10.1016/j.rser.2013.08.097.
[5] McDonough, M., "Integration of Inductively Coupled Power Transfer and Hybrid Energy Storage System: A Multiport Power Electronics Interface for Battery-Powered Electric Vehicles", IEEE Trans. Power Electron., 30(11), pp. 6423–6433 (2015). https://doi.org/TPEL.2015.2422300.
[6] Hannan, M. A., Hoque, M. M., Mohamed, A., et al. "Review of energy storage systems for electric vehicle applications: Issues and challenges", Renewable and Sustainable Energy Reviews, 69, pp. 771–789 (2017). https://doi.org/10.1016/j.rser.2016.11.171.
[7] Campos Rubio, C. V., Kchaou, M., De Faria, P. E., et al. "Development of wind turbines for urban environment using innovative design thinking methodology", Journal of Engineering Research, (2024). https://doi.org/10.1016/j.jer.2024.06.008.
[8] Elalfy, D. A., Gouda, E., Kotb, M. F., et al. "Comprehensive review of energy storage systems technologies, objectives, challenges, and future trends", Energy Strategy Reviews, 54, p. 101482 (2024). https://doi.org/10.1016/j.esr.2024.101482.
[9] Ma, Z. and Sun, D., "Energy Recovery Strategy Based on Ideal Braking Force Distribution for Regenerative Braking System of a Four-Wheel Drive Electric Vehicle", IEEE Access, 8, pp. 136234–136242 (2020). https://doi.org/10.1109/ACCESS.2020.3011563.
[10] Ji, F., Pan, Y., Zhou, Y., et al. "Energy recovery based on pedal situation for regenerative braking system of electric vehicle", Vehicle System Dynamics, 58(1), pp. 144–173 (2020). https://doi.org/10.1016/j.egypro.2019.02.001.
[11] Yu, W., Wang, R., and Zhou, R., "A Comparative Research on the Energy Recovery Potential of Different Vehicle Energy Regeneration Technologies", Energy Procedia, 158, pp. 2543–2548 (2019). https://doi.org/10.1016/j.egypro.2019.02.001.
[12] Raghuwanshi, A. and Ojha, A., "An Overview of the Regenerative Braking Technique and Energy Storage Systems in Electric, Hybrid, and Plug-In Hybrid Electric Vehicles", 2023 IEEE International Students' Conference on Electrical, Electronics and Computer Science (SCEECS), IEEE, Bhopal, India, pp. 1–6 (2023). https://doi.org/10.1109/SCEECS57921.2023.10063062.
[13] Bentouba, S., Zioui, N., Breuhaus, P., et al. "Overview of the Potential of Energy Harvesting Sources in Electric Vehicles", Energies, 16(13), p. 5193 (2023). https://doi.org/10.3390/en16135193.
[14] Yang, C., Sun, T., Wang, W., et al. "Regenerative braking system development and perspectives for electric vehicles: An overview", Renewable and Sustainable Energy Reviews, 198, p. 114389 (2024). https://doi.org/10.1016/j.rser.2024.114389.
[15] Basu, A. and Singh, M., "An Efficient Energy Recovery Approach of a BLDC Driven E-Rickshaw In Regenerating Braking Mode", Scientia Iranica, (2024). H https://doi.org/10.24200/sci.2024.61403.7288.
[16] Geng, C., Ning, D., Guo, L., et al. "Simulation Research on Regenerative Braking Control Strategy of Hybrid Electric Vehicle", Energies, 14(8), p. 2202 (2021). https://doi.org/10.3390/en14082202.
[17] Hosseini, S. M., Soleymani, M., Kelouwani, S., et al. "Energy Recovery and Energy Harvesting in Electric and Fuel Cell Vehicles, a Review of Recent Advances", IEEE Access, 11, pp. 83107–83135 (2023). https://doi.org/10.1109/ACCESS.2023.3301329.
[18] Begum, H. and Hossain, M.A., "Design and Comparison of Vehicle Mounted Wind Turbines", International Journal of Emerging Trends in Engineering Research, 11(1), pp. 1–7 (2023). https://doi.org/10.30534/ijeter/2023/011112023.
[19] Khan, Z. A., Sherazi, H. H. R., Ali, M., et al. "Designing a Wind Energy Harvester for Connected Vehicles in Green Cities", Energies, 14(17), p. 5408 (2021). https://doi.org/10.3390/en14175408.
[20] El, E., Yildiz, C., Dandil, B., et al. "Effect of wind turbine designed for electric vehicles on aerodynamics and energy performance of the vehicle", Thermal Science, 26(4 Part A), pp. 2907–2917 (2022). https://doi.org/10.2298/TSCI2204907E.

[21] Fathabadi, H., "Possibility of Utilizing Wind Turbine to Recover a Portion of the Kinetic Energy Losses of a Car", IEEE Transactions on Vehicular Technology, 68(9), pp. 8663–8670 (2019). https://doi.org/10.1109/TVT.2019.2931192.
[22] Anagie, G. A., Hassen, A. A., and Sintie, Y. T., "Performance Investigation of Small Wind Turbine Installed over a Pick up Vehicle to Charge an Electric Vehicle Battery", JESA, 54(5), pp. 783–788 (2021). https://doi.org/10.18280/JESA.540514.
[23] Ebaid, M. S., Shahin, Z. A. A., and Alshawabkeh, M. M., "Feasibility studies of micro wind turbines installed on electric vehicles as range extenders using real-time analytical simulation with multi driving cycles scenarios", Advances in Mechanical Engineering, 15(4), p. 168781322311659 (2023). https://doi.org/10.1177/16878132231165964.
[24] Nguefack, M. C. F., Fotso, B. E. M., and Fogue, M., "3D numerical investigation of the air flow in the wake of a compact SUV-type vehicle fitted with optimized horizontal Savonius turbines", Journal of the Brazilian Society of Mechanical Sciences and Engineering, 45(1), p. 17 (2023). https://doi.org/10.1007/s40430-022-03933-w.
[25] Schubel, P. J. and Crossley, R. J., "Wind Turbine Blade Design", Energies, 5(9), pp. 3425–3449 (2012). https://doi.org/10.3390/en5093425.
[26] Rosato, A., Perrotta, A., and Maffei, L., "Commercial Small-Scale Horizontal and Vertical Wind Turbines: A Comprehensive Review of Geometry, Materials, Costs and Performance", Energies, 17(13), p. 3125 (2024). https://doi.org/10.3390/en17133125.
[27] Yildiz, A. and Dandil, B., "Power Generation Potential of Small Wind Turbine in Elazig Province, Turkey", 2019 4th International Conference on Power Electronics and Their Applications (ICPEA), IEEE, Elazig, Turkey, pp. 1–6 (2019). https://doi.org/10.1109/ICPEA1.2019.8911158.
[28] Bashir, M. B. A., "Principle Parameters and Environmental Impacts that Affect the Performance of Wind Turbine: An Overview", Arabian Journal for Science and Engineering, 47(7), pp. 7891–7909 (2022). https://doi.org/10.1007/s13369-021-06357-1.
[29] Bilgili, M., Tumse, S., Tontu, M., et al. "Effect of Growth in Turbine Size on Rotor Aerodynamic Performance of Modern Commercial Large-Scale Wind Turbines", Arabian Journal for Science and Engineering, 46(8), pp. 7185–7195 (2021). https://doi.org/10.1007/s13369-021-05364-6.
[30] Bayron, P., Kelso, R., and Chin, R., "Experimental investigation of tip-speed-ratio influence on horizontal-axis wind turbine wake dynamics", Renewable Energy, 225, p. 120201 (2024). https://doi.org/10.1016/j.renene.2024.120201.
[31] Schaffarczyk, A. P., "Basic Fluid Mechanics", In Introduction to Wind Turbine Aerodynamics, Springer International Publishing, Cham, pp. 27–72 (2020). https://doi.org/10.1007/978-3-030-41028-5_3.
[32] Deda Altan, B. and Gungor, A., "Improvement of Savonius wind turbine performance with using wind collector", Scientia Iranica, 31(13), pp. 1020–1029 (2023). https://doi.org/10.24200/sci.2023.60454.6809.
[33] Jureczko, M., Pawlak, M., and Mężyk, A., "Optimisation of wind turbine blades", Journal of Materials Processing Technology, 167(2–3), pp. 463–471 (2005). https://doi.org/10.1016/j.jmatprotec.2005.06.055.
[34] Bak, C., "Sensitivity of Key Parameters in Aerodynamic Wind Turbine Rotor Design on Power and Energy Performance", J. Phys.: Conf. Ser., 75, p. 012008 (2007). https://doi.org/10.1088/1742-6596/75/1/012008.
[35] Hau, E., "Rotor Aerodynamics", In Wind Turbines, Springer Berlin Heidelberg, Berlin, Heidelberg, pp. 89–166 (2013). https://doi.org/10.1007/978-3-642-27151-9_5.
[36] Yin, R., Xie, J.-B., and Yao, J., "Optimal Design and Aerodynamic Performance Prediction of a Horizontal Axis Small-Scale Wind Turbine", Mathematical Problems in Engineering, 2022, pp. 1–19 (2022). https://doi.org/10.1155/2022/3947164.
[37] NACA-0009 9.0% smoothed (n0009sm-il), (n.d.). http://airfoiltools.com/airfoil/details?airfoil=n0009sm-il (accessed August 28, 2023).
[38] Gasch, R. and Twele, J., "Blade geometry according to Betz and Schmitz", In Wind Power Plants, R. Gasch and J. Twele, Eds., Springer Berlin Heidelberg, Berlin, Heidelberg, pp. 168–207 (2012). https://doi.org/10.1007/978-3-642-22938-1_5.

FIGURE CAPTIONS

TABLE CAPTIONS

FIGURES

Figure 14. Cross section of an airfoil [31]

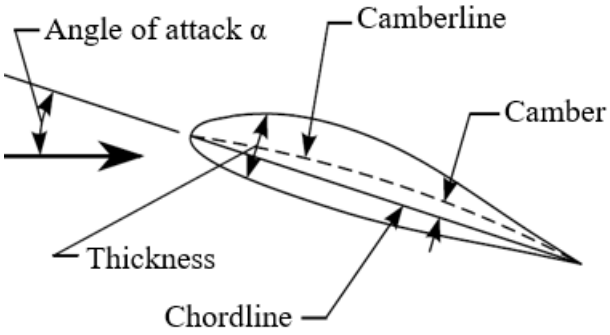

Figure 15. Geometric airfoil parameters of the NACA airfoil series [35]

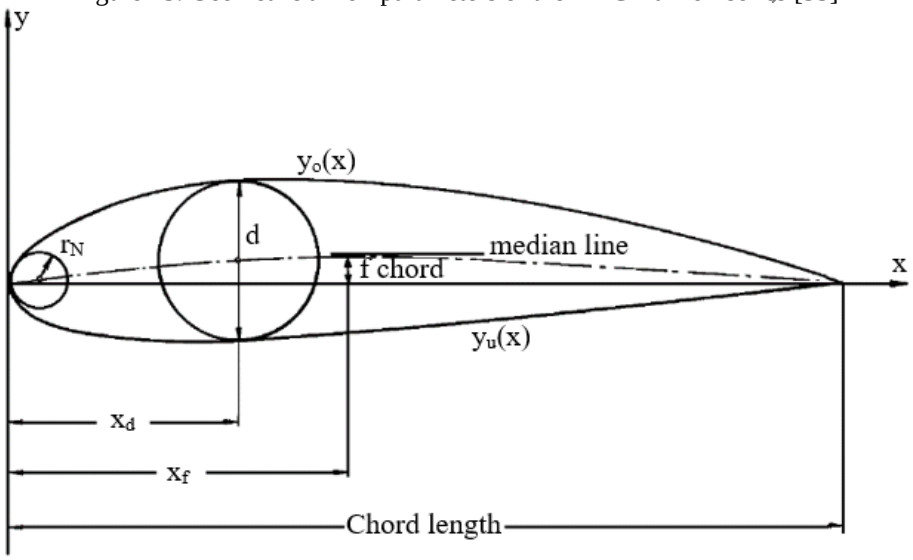

Figure 16. NACA0009 airfoil [37]

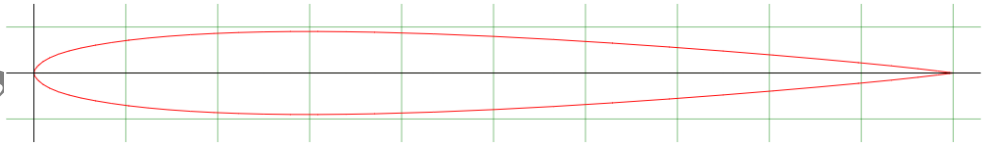

Figure 17. Section points and their distances to the blade root

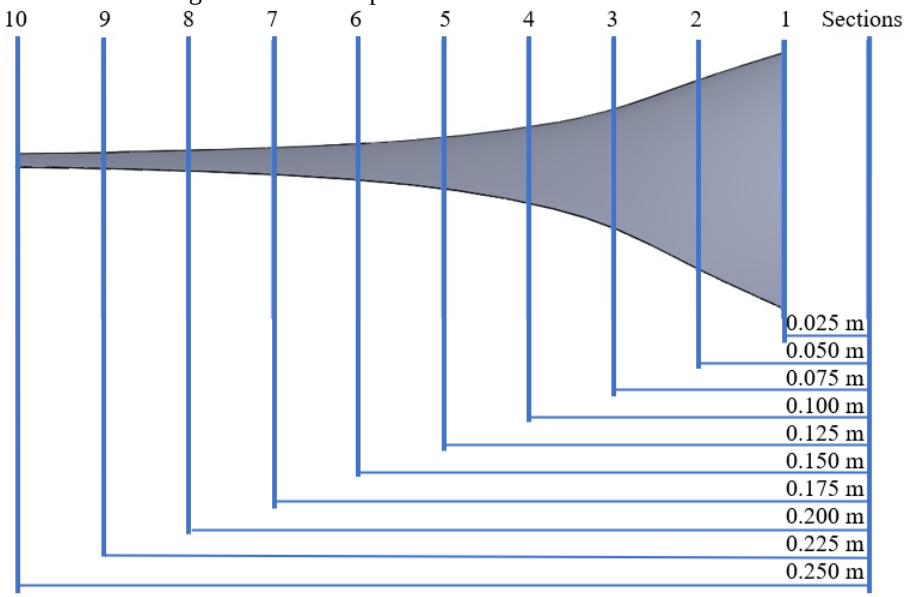

Figure 18. Front view of airfoils at different sections

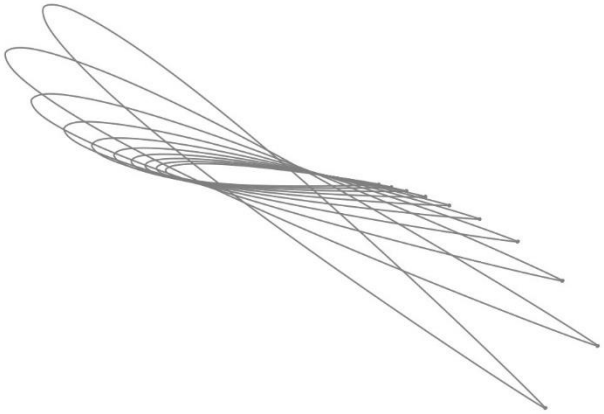

Figure 19. a. Isometric view of airfoils at different sections, b. Rootless blade solid model

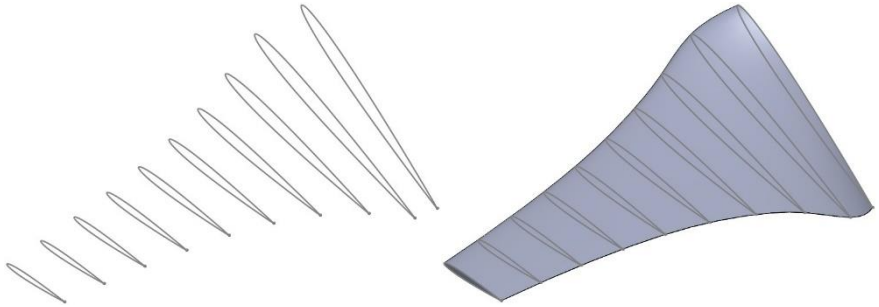

a **b**

Figure 20. Model of the three-bladed turbine

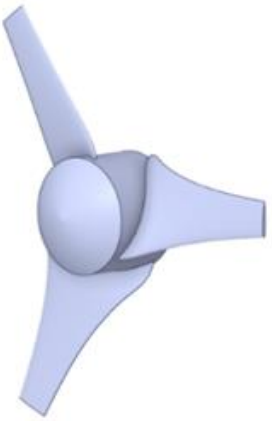

Figure 21. Computational domain of numerical simulation

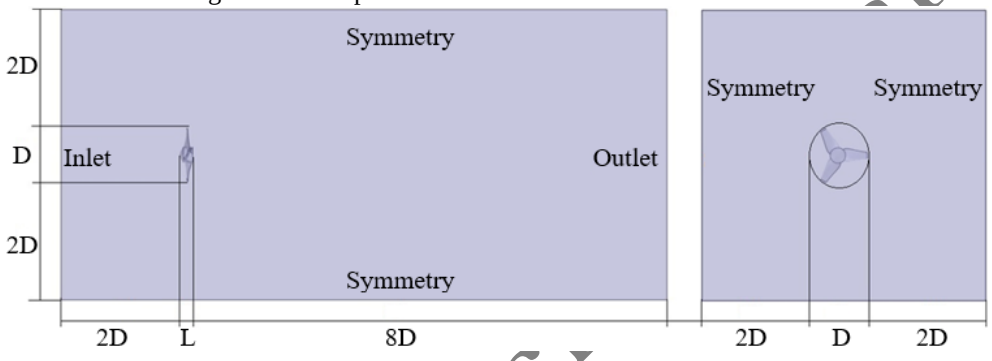

Figure 22. Triangular mesh structure of the model

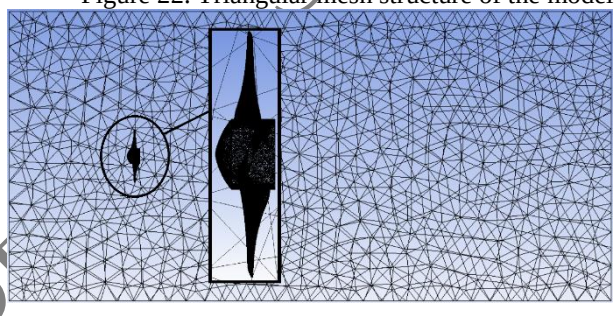

Figure 23. Representation of the medium-density mesh with 3678920 elements

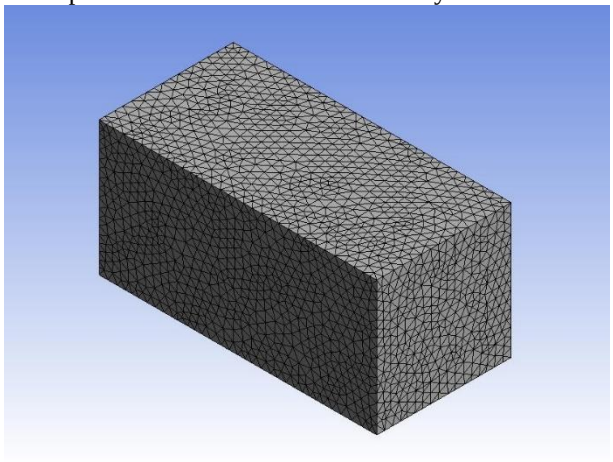

Figure 24. Static pressure contours on turbine blades at different wind speeds

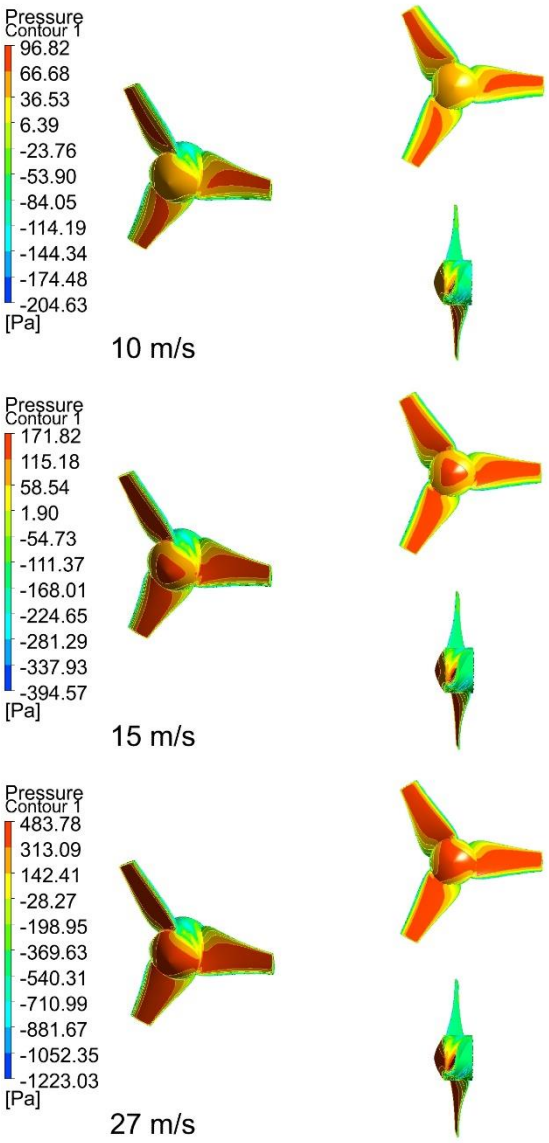

Figure 25. Velocity distribution on turbine blades at different wind speeds.

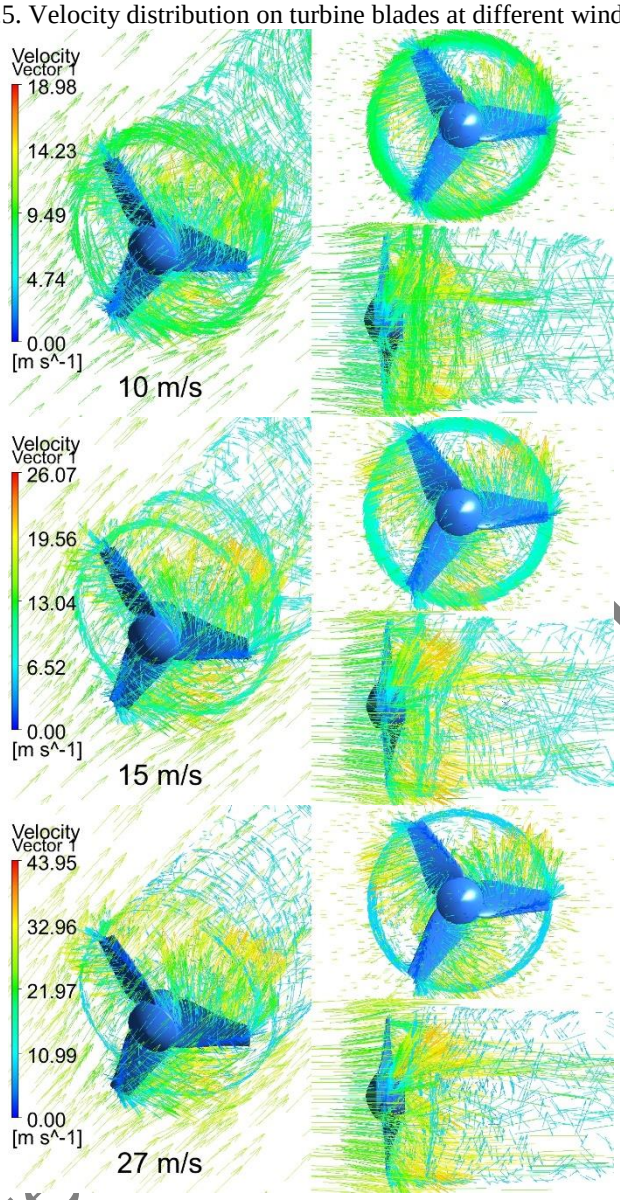

Figure 26. Streamlines on turbine blades at different wind speeds

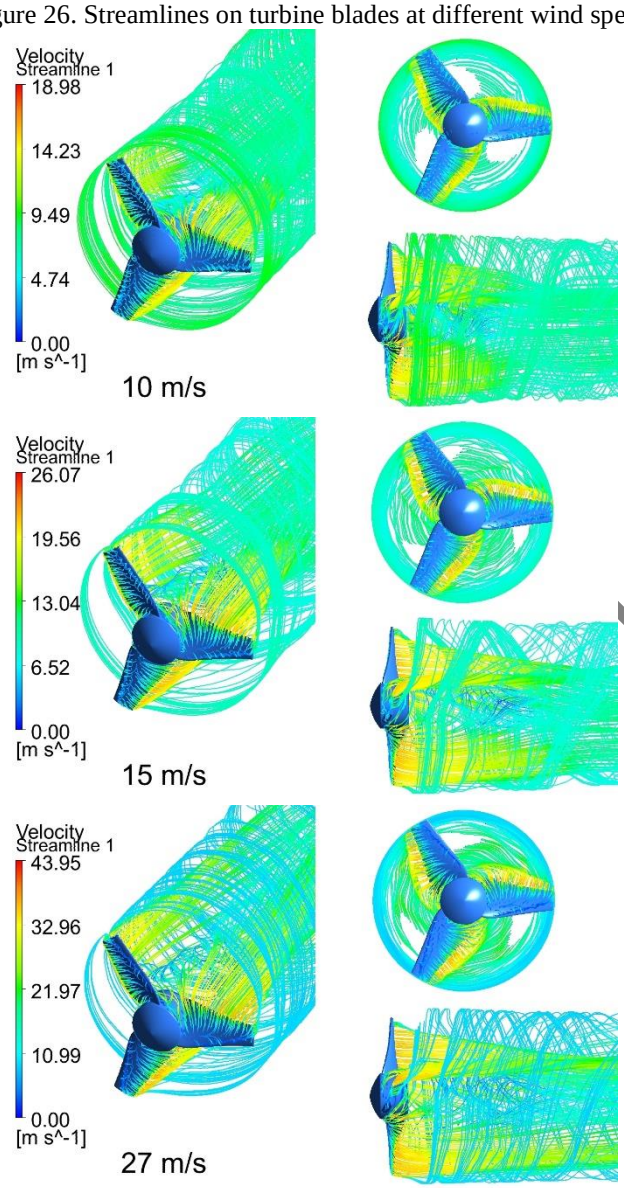

TABLES

Table 4. C_l/C_d ratio change according to the angle of attack of NACA0009 airfoil

The angle of attack α	C_l	C_d	C_l/C_d
3.25	0.4104	0.00909	45.14851
3.50	0.4332	0.00947	45.74446
3.75	0.4557	0.00992	45.9375
4.00	0.4781	0.01043	45.83893
4.25	0.5001	0.01105	45.25792

Table 5. A result of the calculations, blade twist angles and chord lengths

Sections	r (m)	β (r)	C (r)
1	0.025	38.54	0.1196
2	0.050	26.25	0.1232
3	0.075	18.72	0.1046
4	0.100	13.97	0.0872
5	0.125	10.79	0.0736
6	0.150	8.54	0.0632
7	0.175	6.89	0.0553
8	0.200	5.61	0.0490
9	0.225	4.61	0.0439
10	0.250	3.79	0.0398

Table 6. The reference values, boundary conditions, and solution settings used in wind turbine analyses.

Reference values		
1	Dynamic viscosity	1.789×10^{-5} Pa x s
2	Density	1.225 kg/m^3
Boundary Conditions		
1	Velocity inlet	10 m/s, 15 m/s, 27 m/s
3	Pressure outlet	Atmospheric pressure
4	Side and top outlet	Symmetry
5	Fluid type	Air
6	Turbulence intensity	5%
7	Viscosity ratio	10%
Solution Settings		
1	Turbulence Model	SST k-omega
2	Pressure	Second order
3	Momentum	Second order upwind
4	Turbulence kinetic energy	Second order upwind
5	Turbulence dissipation ratio	Second order upwind